Biosensors and Bioelectronics 85 (2016) 522–528

Contents lists available at ScienceDirect

Biosensors and Bioelectronics

journal homepage: www.elsevier.com/locate/bios

Development of SERS substrate using phage-based magnetic template for triplex assay in sepsis diagnosis

Anh H. Nguyen [a], Yesol Shin [a], Sang Jun Sim [a,b,*]

[a] Department of Chemical and Biological Engineering, Korea University, Seoul 136-713, Republic of Korea
[b] Green School, Korea University, Seoul 136-713, Republic of Korea

ARTICLE INFO

Article history:
Received 2 March 2016
Received in revised form
3 May 2016
Accepted 13 May 2016
Available online 14 May 2016

Keywords:
SERS-tags
Sepsis
Biosensor
Plasmonic nanoparticles
Mesoporous materials
Multiplex detection

ABSTRACT

Development of a new substrate for surface-enhanced Raman scattering (SERS) is one area of interest for the improvement of SERS performance. Herein, we introduce a new method for developing new mesoporous SERS substrates using M13 phages that display cysteine-rich peptides on the pVIII major units, which is an alternative for thiol donor using chemical modifications. Together with the SERS substrate development, and the use of the SERS technique for sepsis diagnostics is a new approach in clinical settings. The substrates were characterized and magnetized with magnetic immuno colloids made of gold-coated magnetic nanoparticles and specific antibodies. Conventionally, the SERS-tags are prepared by using gold nanoparticles and are modified with Raman dyes to immobilize specific antibodies to capture the biomarkers in the serum samples. However, in this method the SERS-tags are bound to the mesoporous substrate via antibody/antigen interactions to form clusters or layer-by-layer assemblies of SERS-tags for Raman signal enhancement. The SERS spectra showed distinct peaks for tags corresponding to three typical sepsis-specific biomarkers for diagnostics with the limit of detection values of 27 pM, 103 pM, and 78 pM for C-reactive protein (CRP), procalcitonin (PCT), and soluble triggering receptor expressed on myeloid cells-1 (sTREM-1), respectively. With such an approach, SERS can be used for clinical purposes and can be improved by phage display modification rather than chemical alternatives.

1. Introduction

Mesoporous materials are materials with the diameters of pores between 2 and 50 nm (Groen et al., 2003). Due to this property, nanoparticles have been inserted inside the mesopores to achieve new functions, such for bio/chemical catalysis (Vera-Robles et al., 2015) and imaging (Ghosh et al., 2012). However, the application of nanoparticle-embedded mesoporous templates as a substrate for surface-enhanced Raman scattering (SERS) has not been reported elsewhere. Mesoporous materials can be synthesized in two ways: (i) one-step mesostructure synthesis with simultaneous functionalization (Huang et al., 2008) and (ii) macro-biomolecule-based templates and scaffolds to create mesoporous materials (Zhang et al., 2002). However, unlike the second way, the first way faces several limitations with the self-assembly of surfactant molecules that affect the yield of a homologous structure. The second way shows considerable capacity for mesostructure synthesis because of features such as a definite structure and size monodispersity using chemical bioconjugation. Among biomaterial templates, M13 bacteriophage can be considered as a potential biomaterial template for the synthesis of mesoporous templates because it's outstanding chemical nature of the M13 bacteriophage such as self-assembly and orchestrated phage-based materials in combination with other metallic nanostructures (Blaik et al., 2016). Moreover, functionalization of the M13 bacteriophage with particular functional groups improves the properties of M13 for template fabrications (Li et al., 2010) and phage-based diagnostic method (Swift et al., 2013). In previous studies, the surface of phages had to be treated with thiol-donor substrates to introduce nanoparticles into the phage templates (Vera-Robles et al., 2015; Chung et al., 2014). However, this process requires a chemical modification in the entire phage structure and results in denaturation of the phage surface that can affect its natural characteristics such as assembling and binding. To overcome this, phage display can be used to express the functional groups (e.g. thiol moieties) instead of chemical modifications on M13 phage. In principle, a M13 filamentous bacteriophage consists of a long rodlike shape, 800–900 nm in length and 6.5 nm in diameter.

* Corresponding author at: Department of Chemical and Biological Engineering, Korea University, Seoul 136-713, Republic of Korea.
E-mail address: simsj@korea.ac.kr (S.J. Sim).

http://dx.doi.org/10.1016/j.bios.2016.05.043
0956-5663/

Entire phage body is covered by a major coat protein pVIII with 2,700 copies and each end has two minor coat proteins (pVII, pIX and pVI, pIII) with 3–5 copies (Smith, 1985). Coat proteins are coded by the phage genome, which reflects a direct link between the genotype and phenotype. Coat proteins pVIII and pIII are generally selected for peptide displays because the genes contain N-terminal perisplasm-directing signal sequences to overcome protein aggregation. The outstanding biochemical properties of phage were applied in various fields. Phages have been fabricated for superior building blocks that have been applied in sensors and photovoltaic cells by combination with other organic/inorganic substances. Besides utilizing chemical functionalization, genetic engineering can also be a potential tool to improve the efficiency of a more densely packable unit size of phage, and a self-template block. A practical application is optical-based sensors which are developed with display of target-specific binding motifs on the phage-coat proteins. Thus, the self-templating feature may contribute the field of either plasmonic phenomena or SERS substrates.

Plasmonic nanoparticles can overcome the drawbacks of fluorescent techniques (Sharma et al., 2012). Because plasmonic metallic nanoparticles consist of electromagnetic oscillations at their surfaces and localized resonant excitations, they amplify the electromagnetic fields that support electromagnetic SERS enhancement. The SERS spectra of an analyte is strongly enhanced (10^9–10^{11} folds) if it is absorbed onto the nanoparticle surface (chemical mechanism) or located in the plasmonic band of nanoparticles (electromagnetic mechanism). In experiments, SERS substrate is the first choice of consideration for optimal SERS performance. The substrates were fabricated using the bottom-up (Sharma et al., 2013) or top-down methods (Abu Hatab et al., 2008) according to the research purpose and the laboratory facility. In the bottom-up method, nanorods (Tsvetkov et al., 2013), nanostars (Nguyen et al., 2015a), and nanospheres (Joseph et al., 2011) are used to build block, layer-by layer structures of hot-spot enhancements. With this design, the substrates have tunable plasmon resonance properties and average enhancement factors which are reciprocal at a distance to the substrate surface. Moreover, the success of SERS is strongly dependent on the interaction between the analytes and the SERS substrates (Sharma et al., 2012). SERS-based diagnostics have been applied in the detection of various cancers, Alzheimer's disease, virus infection (Huh et al., 2009; Yang et al., 2015), and DNA modifications (Nguyen et al., 2015a).

Sepsis has a rather high mortality rate and has been called as an unseen public disaster (Rittirsch et al., 2008). It is caused not only by the infecting pathogen but also by the inflammatory response to the infection, which can be immediately septic and damage to tissue and organ systems (Reinhart et al., 2012; Rittirsch et al., 2008; Rascher et al., 2014). Specifically, sepsis causes immediate multiple-organ failure; early and accurate diagnostics for immediate treatment is required. The accurate and timely detection of sepsis still remains as a challenge. Herein, we describe the fabrication of new SERS-based diagnostics for sepsis using the designed SERS substrate. For direct diagnostics of pathogens, the limitations of blood culture are time consuming, low sensitivity (only 30%) and inability to culture 30% of infected bacteria (Calandra and Cohen, 2005). Some methods involving the use of multiplex real-time PCR for the identification of blood stream pathogens yield false negatives because patients without suspicion of infection do not have bacterial DNA in their blood (Sutherland et al., 2011). As an alternative, molecular diagnostics of sepsis-specific biomarkers have been considered. However, no single detection method for only one specific biomarker has yet been determined with the high sensitivity and specificity, so another approach is to use a panel of biomarkers in clinical settings (Gibot et al., 2012). Three biomarkers including C-reactive protein, procalcitonin, and sTREM-1 have been approved for sepsis diagnostics (Zakariah et al., 2008). A biomarker-based multiplex assay with the sensitivity and specificity would be considered for early sepsis detection.

Herein, we report the development of SERS substrates based on plasmonic mesoporous template for sepsis detection. The structures are synthesized by the phage display of cysteine-rich peptide on pVIII domain of the M13 for the template fabrication. The cysteine moieties in the mesoporous templates are reduced into the active thiol groups that are highly condensed binding to gold-coated magnetic nanoparticles for formation dual properties of plasmonic coupling-based SERS enhancement and magnetic template for separation. The structures are used as SERS substrates for triplex detection of sepsis based on principles of immunoassays. For preparation of optical reporter, SERS-tags were prepared by bioconjugation of the specific antibodies and Raman dyes onto the nanoparticle surface. A SERS-based sandwich immunoassay for the triplex assay of sepsis-specific biomarkers including CRP, PCT, and sTREM-1 were then performed on the magnetic plasmonic templates in human serum. A resultant was separated by a magnet and then used for SERS measurement. The triplex assays of CRP, PCT and sTREM-1 showed good specificity, high sensitivity and relatively low detection limits, which indicates that the SERS-based assay can be used for alternative assays for monitoring the early stages of sepsis.

2. Experimental section

2.1. Construction of pVIII-displayed cysteine-rich peptide using M13KE

The sequence of the pVIII major DNA of M13KE was retrieved from the database of DNA maps and DNA sequences and Maps Tool of New England Biolabs (NEB). We displayed a cysteine-rich peptide (GBSI01000616.1) on the pVIII protein to generate a thiolated phage with a simple reaction of 0.05 M tris (2-carboxyethyl) phosphine hydrochloride solution (TCEP) for 30 min Phage strains (M13KE, F´*proA*$^+$*B*$^+$ *lacI*^{q} Δ*(lacZ)M15zzf*) were used as a core for the insert construction. XL-10 gold ultracompetent cells (*F′ lacI*^{q} *ZΔM15*) (Aligent genomics) were used to transform the ligated DNA product. *E.coli* (ER2738) from NEB was used for phage amplification.

The cysteine-rich peptide motifs on every copy of the pVIII major coat protein were cloned by a polymerase chain reaction (PCR). PCR was performed with a couple of primers: aaagcgatgATGCCCAAGTGCCCTCG (gcgatg: BtgZI site) and aaagcgcATTGAAAGTGTAGCTTTC (gcgc: HinP1I site) and the PCR products were digested with BtgZI (10 units/μl) and HinP1I (10 units/μl). The M13KE vector was digested with the same enzymes used to prepare the insert. The inserts were ligated into the vector with T4 DNA Ligase. The DNA sequence of the peptides was inserted into the genome of the wild-type pVIII at specific residues ((position 1301…1522), refer to DNA maps and sequences of NEB). The recombinant phages as blue plagues were selected on LB/IPTG/Xgal plate. The recombinant DNA was isolated using commercial isolation kits (Qiagen, USA) and sequenced by a sequencing service. The products (3 μl) were transformed into 100 μl of XL-10 gold ultracompetent cells to select the blue plaques on the LB/IPTG/Xgal plates. The recombinant phages were amplified in ER2783 at 37 °C for 5 h. The cell suspension was centrifuged for 20 min at 4 °C. The phages from the supernatant were twice precipitated with 20% PEG/2.5 M NaCl (ratio 1:6). The phages displaying cysteine-rich peptides were resuspended in tris-buffered saline for storage and further use.

2.2. Development of SERS substrate for sepsis detection

Production of thiolated phages were described in the supporting method S3. To produce magnetic templates, 500 μl phages was treated with 300 μl of silica precursor tetraethyl orthosilicate (TEOS) and (3-aminopropyl) triethoxysilane (APTES) with a molar ratio of 10:1 for 60 min The templates were then calcinated at 600 °C for 4 h to form the thiol phage-silica mesoporous template. The template was magnetized and obtained plasmonic property by fabrication with 100 μl of 75 mM gold-coated magnetic immunogold colloids (see Supporting method S4). The protocol for the antibody conjugation was presented in Supporting method S5. The templates were washed three times with phosphate-buffered saline (PBS) through a gentle centrifugation (1500 rpm) and the templates were then isolated by a magnet. Finally, the templates were stored in PBS at 4 °C for further use as SERS templates. The SERS templates were characterized with TEM (JEM-2100F, Jeol 200 kV), UV–vis–NIR spectrophotometer (UV-3600, Shimadzu) and EDX. The magnetic templates were then ready to capture the SERS tags on their surface for SERS scanning.

2.3. Triplex detection of sepsis-specific biomarkers

The recombinant biomarkers including CRP, PCT, and sTREM-1 ranging from 1 pM to 1 nM were prepared in 1 ml commercial human serum (H4522, Sigma) to mimic real serum samples. 50 μl of 1 mM SERS-tags for each corresponding target antigen was added at 0.5 ml above the serum and incubated for 30 min with gentle mixing. The samples were spun to collect the complexes of the target biomarkers bound onto the surface of SERS-tags and the free targets in the supernatant were eliminated. The pellets were washed three times with PBS to completely remove the free biomarkers. 200 μl suspensions of the magnetic templates were added to the pellets to form a complex of magnetic complex-biomarker-SERS-tags. The complexes were separated from the suspension using the DynaMag™−2 Magnet (12321D, Invitrogen) and washed three times with PBS before SERS measurement. The limit of detection (LOD) for the SERS assay was calculated using the reported formula (Nguyen et al., 2015b) based on specific fingerprinting peaks of Raman spectra. A control experiment was performed with 500 μl of (2 mg/ml) human serum albumin (HSA), 2 mg/ml bovine serum albumin (BSA) and the commercial human serum (H4522, Sigma).

3. Results and discussion

3.1. Synthesis of phage-based mesosporous magnetic template

Cysteine-rich peptide (243 bp) displaying phages (see supporting method S1 and S2) were constructed by using a wild type M13KE of pH. D.™-12 phage display kit (New England Biolabs). The target was inserted between a pVIII start codon and a leader peptide (Fig. 1(A)) by using two restriction enzymes BtgZI and HinP1I. The peptide (MKKSLVLKASVAVATLVVPMLSFA) was inserted to ensure correct folding of the cysteine-rich peptide and displayed on the phage surface (Fig. 1(A)). The resulting construct was transformed into XL-10 gold ultracompetent cells with an unmodified construct M13KE as negative control. The successful transformation was confirmed by colony PCR and sequencing. Fig. 1(B) shows the DNA electrophoresis results for the colony PCR products of the recombinant constructs with ~243 bp longer fragment (lane 2 (clone 1), lane 3 (clone 2) and wild type M13KE (lane 4). The recombinant phage bearing XL-10 gold cells was cultured to produce the phage particles. The phage particles were collected by incubating twice with PEG/2.5 M NaCl at 4 °C overnight. The pure particles were transfected into ER2738 *E.coli* overnight for amplification of the phage particles. The phages collected by the above method were used for development of the magnetic template by a simple 5% TCEP treatment (see Supporting method S3).

The schematic illustration of the development SERS magnetic template is presented in Fig. 1(C). After treatment with TCEP to generate the active thiol groups, the phages were treated with 150 μl of a silica precursor mixture of TEOS/APTES (10:1 M) (Vera-Robles et al., 2015). The phages self-assembled in the liquid-crystal structures at 2.0 mg/ml and then polymerized into amorphous silica white powders with silicalization of the silica precursors (Fig.

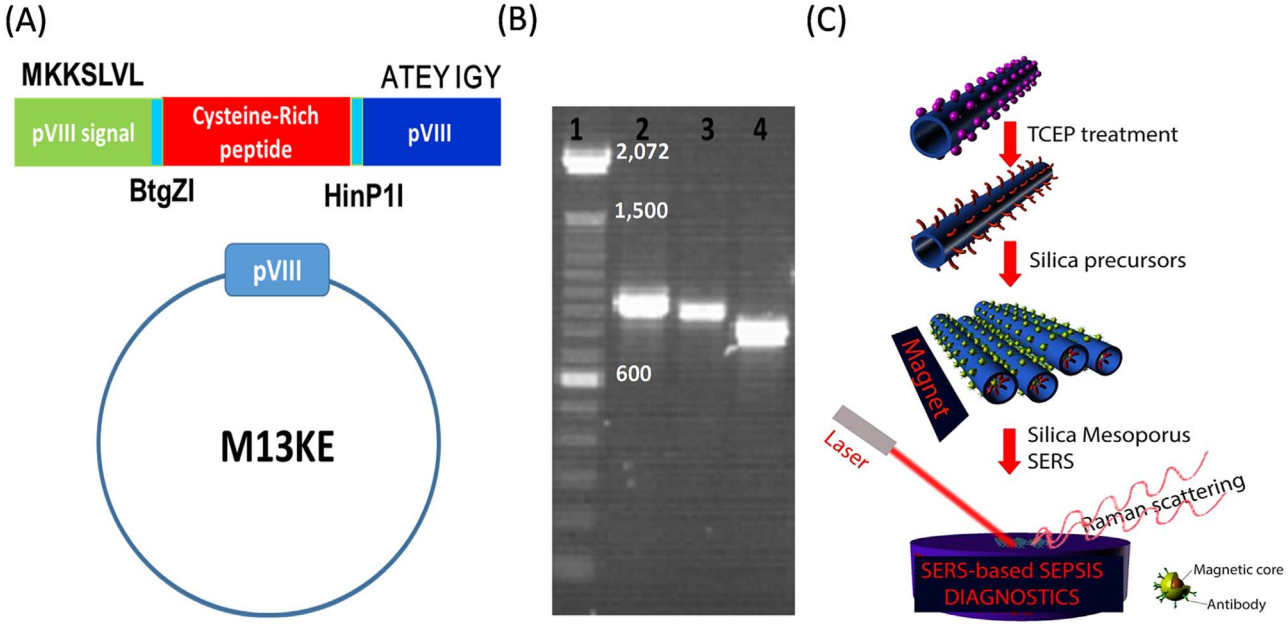

Fig. 1. Schematic illustration from phage display to fabrication of SERS substrate. (A) Insertion of cysteine-rich peptide into pVIII domain. (B) Colony PCR on 1% agarose gel indicates the successful insertion of cysteine-rich peptide into pVIII of M13KE. Lane 1, 100 bp marker (cat. no. 15,628–019); lane 2 and lane 3, recombinant of M13KE; lane 4, wild type of M13KE. (C) Scheme of using cysteine-rich peptide phage display for SERS substrate fabrication.

S1). Similarity with chemical thiolation of the phages (Vera-Robles et al., 2015), the thiol-template derived silica oxide mesoporous network, was obtained after adding the TEOS/APTES mixture with morphology transitions from a turbid suspension to a white gel after 30 min To complete the hydrolysis-condensation of the precursors, the gel was incubated in the incubator at 55 °C for 24 h and then washed and dried at ambient temperature. The products were finally calcined at 600 °C for 3 h, Si-O framework formation on the phage biotemplate produces the mesoporous structures. Thiol groups in the mesoporous template were qualified by FTIR spectroscopy. FTIR spectra of the template at various stages of its modification by thiolation functionalization and calcination were performed to monitor changes on its surface. The spectra clearly showed that the thiol groups did not disappear during calcination process due to the presence of the weak S-H vibrations at 2580 cm^{-1} (Oh et al., 2006) in all three stages of the samples. (Fig. S3). The existing of silica precursor in the functionalized template was evidenced by the presence of strong Si-O stretching vibration at 1358 cm^{-1} (Tian et al., 2010). The weak –SH peak at 2580 cm^{-1} in the calcinated template indicates that the calcination at 600 °C did not degrade –SH moieties during calcination stage. The thiol moieties provided anchoring sites for binding gold nanoparticles on the mesoporous templates.

3.2. Synthesis of gold-coated magnetic nanostars and preparation of immunogold colloids

Gold-coated magnetic nanostars (Au-MNS) (Fig. 2(A)) were synthesized by the seeded growth method. Briefly, 20-nm AuNP (Fig. 2(B)) were dispersed in 0.2 M CTAB and then added to a growth solution containing 0.2 M CTAB, 10 mM $HAuCl_4$ and 100 mM $AgNO_3$ and 0.25 mM sodium citrate to produce 35 nm nanostars with tip-to-tip and tip-to-core plasmonic resonance. The visible spectra of AuNP (596.7 nm) and Au-MNS (653.8 nm) are shown in Fig. 2(C). The CTAB and citrate residues on the surface of the Au-MNS and AuNPs were exchanged with a mixture of 0.1 mM OEG6: OEG3 (1:3). The unspecific sites were then blocked with 1% BSA in phosphate-buffered saline and stored at 4 °C for antibody conjugation.

Raman dyes-bound immunogold colloids, called SERS-tags, were produced by a typical EDC/NHS bioconjugation (see Supporting method S3). The wavelength shifted from 596.7 nm to 608.2 nm and from 653.8 nm to 667.1 nm corresponding to bioconjugation of the specific antibodies to the AuNP and Au-MNS surfaces, respectively (Fig. 2(C)). Plasmonic damping due to antibody functionalization on the nanoparticle surface is 11.5 nm and 13.3 nm for AuNPs and Au-MNS respectively (Fig. 2(C)). Since the distinct absorption peak from the surface plasmon of the AuNPs or Au-MNS is a result of a collective excitation of electrons at the interface between the conductor and insulator. Binding of antibody on the nanoparticle surface alters its surface plasmon properties and increases refractive index on the nanoparticle surface, which results in the red-shift spectra of surface plasmon resonance, is the basis of label-free SPR biosensing (Nguyen et al., 2015c; Brolo, 2012; Hall et al., 2011). Moreover, no agglomeration was observed with phenomena such as broadening of adsorption peaks and a decrease in peak intensity during process of antibody conjugation.

3.3. Generation of magnetic phage template for sepsis diagnostics

In order to generate the active thiol group, the phage displaying cysteine-rich peptide was treated with 0.05 M TCEP. Thiolated phage templates were then decorated by Au-MNS to form a magnetic phage template. The thiol quantification of the thiolated phages was described in the Supporting method S6 and the result was shown in Fig. 3(A). The recombinant phages were composed of more cysteine disulfide moieties than the wild-type phages due to the cysteine phage display. The thiolated phages were polymerized with a mixture of silica precursors (TEOS/APTES) to create amorphous gel (Fig. S1). Then, the amorphous gel was calcinated at 600 °C for 4 h and the silica mesoporous formation was detected by Raman spectra. The Raman spectra of the silica mesoporous structures are shown in the frequency shift region extending from 200 to 2500 cm^{-1} with a peak at 547.9 cm^{-1} (Fig. 3(B)). These spectra assign distinct peaks that can be attributed to the motions of Si and O atoms within the mesoporous structures of the tetrahedrally derived phages (Kingma and Hemley, 1994). Weak peaks around 600 cm^{-1} correspond to Si-O stretching modes, while the peak at 368 cm^{-1} correlates with the O-Si-O bending modes.

Based on the SERS principle (Sharma et al., 2012), close proximity of Au-MNS increases the electromagnetic field that promotes SERS intensity in SERS-based diagnostics. The mesoporous templates were decorated with immunogold Au-MNS (Fig. 4(A)). The immunogold colloids were bound to the thiolated template to form coupled or clustered nanoparticles on the template surface. The coupled nanostructures enhance the electromagnetic coupling between gold nanoparticles that can increase the intensity of Raman spectra for the probe molecules. Moreover, the cavities in mesoporous structures hold the immunogold nanoparticles to

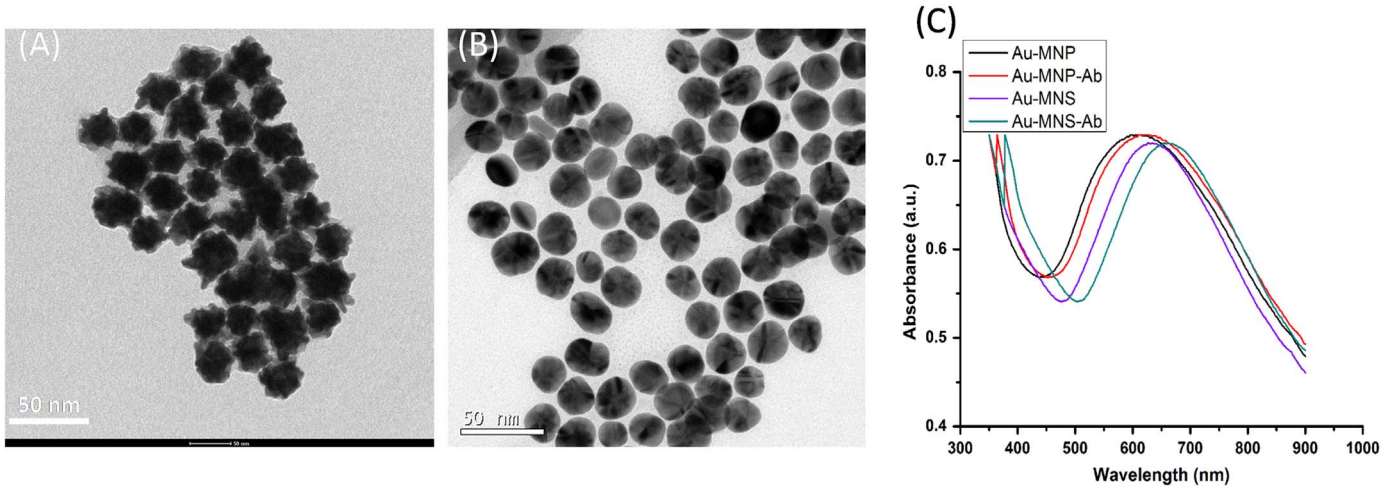

Fig. 2. Characterization of the gold nanoparticles (AuNPs) and gold-coated magnetic nanostars (Au-MNSs). (A) TEM image of AuNP. (B) TEM image of Au-MNS. (C) UV/Vis spectra of bare AuNPs and Ab-functionalized AuNPs.

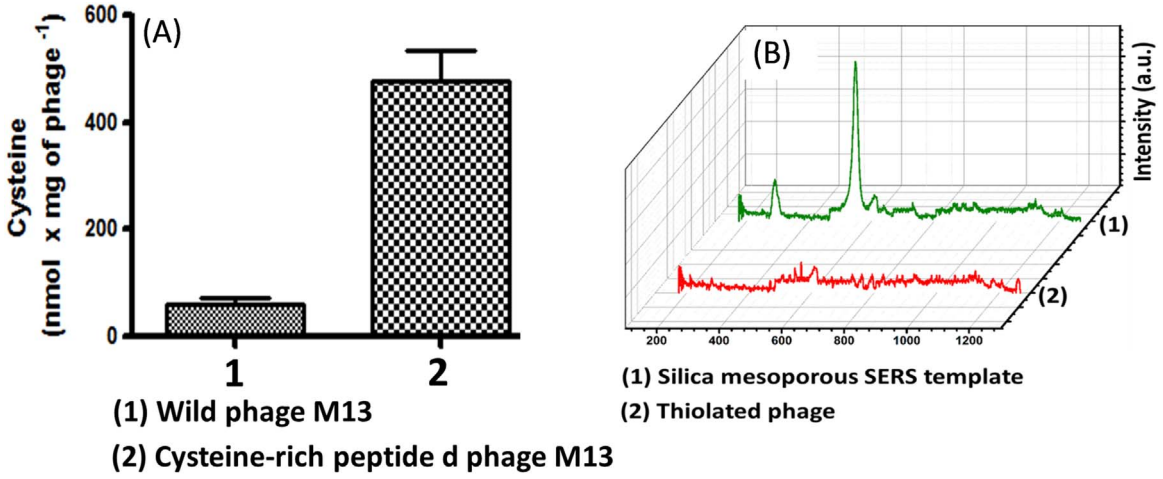

Fig. 3. Characterization of the mesoporous SERS templates. (A) Quantification of cysteine-based thiol groups on the surface of recombinant and wild M13 phages. (B) Raman spectra of the SERS substrate.

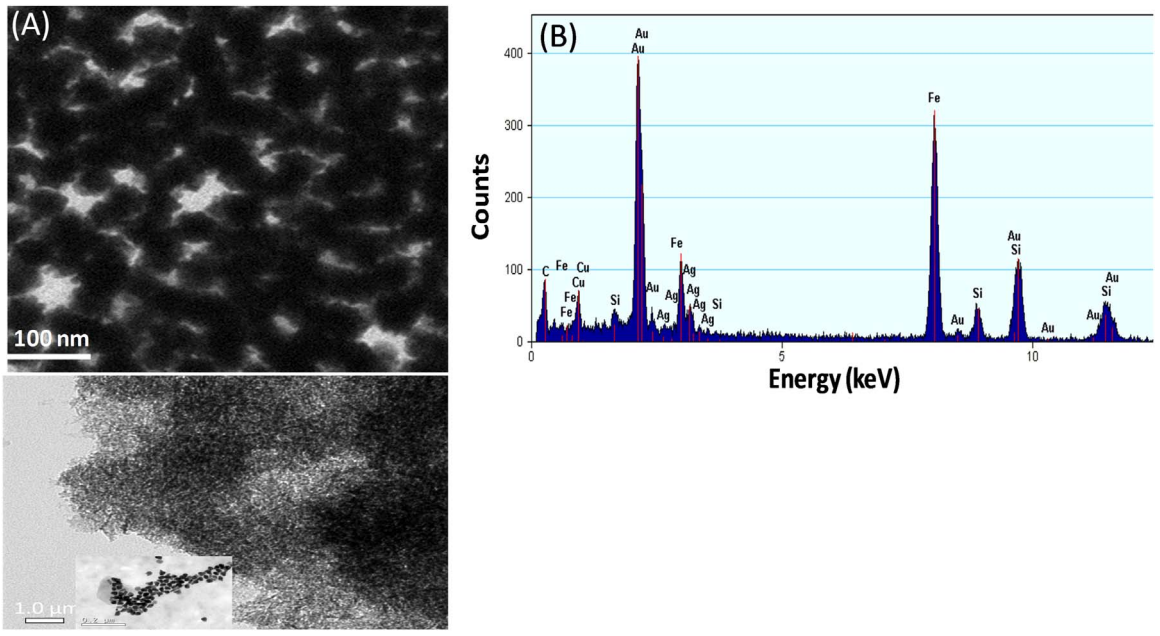

Fig. 4. Fabrication of the SERS template by binding Au-MNS into thiolated phage. (A) Distribution of Au-MNS on the magnetic template at 100 nm scale (upper) and Au-MNS binding to the thiolated phage template via thiol-gold atom interactions (below). (B) EDX analysis of mesoporous SERS-templates.

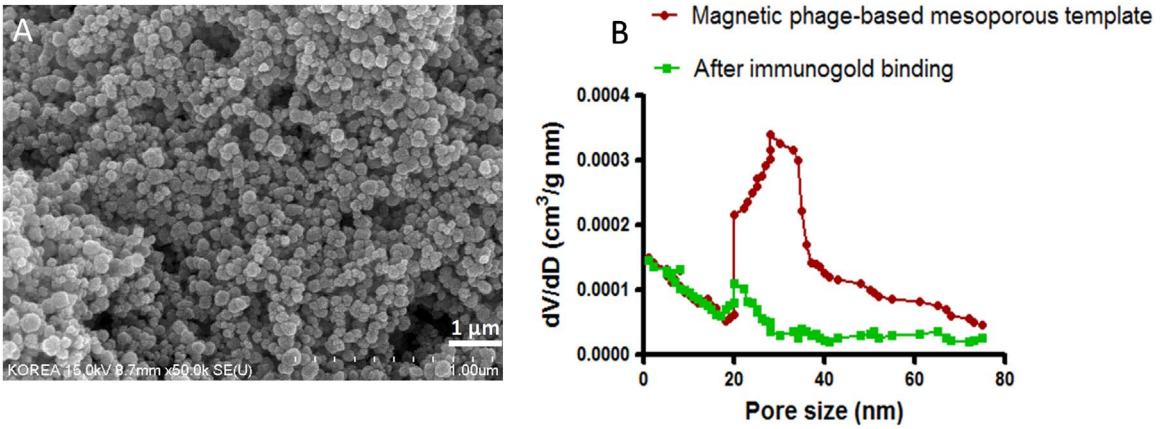

Fig. 5. Surface of the mesoporous SERS templates when immunogold colloids recognizing target biomarkers. (A) SEM image of the mesoporous SERS template after immunogold colloids binding to the template. (B) Pore size of the magnetic phage-based mesoporous template and after the immunogold binding to the template.

increase enhancement of SERS performance (Nguyen et al., 2015b). The atoms of the templates were characterized by Energy-dispersive X-ray spectroscopy (EDX) that results in Fe, Au, and Si presenting in the template (Fig. 4(B)). Similarly, the physical properties of the templates generated from the cysteine-rich peptide displaying phages are similar to those from thiol-donor substrate based methods (Vera-Robles et al., 2015; Chung et al., 2014). TEM image (Fig. 4(A)) showed the templates-decorated Au-MNPs resulted in highly condensed structures of close proximity. Likewise, thiol groups and tyrosine or phenylalanine residues in the pVIII units serve as nucleation sites for growth of metallic atoms by a reducing agent, which can exploit for SERS enhancement (Nguyen et al., 2015b; Pokorski and Steinmetz, 2011).

The pore sizes on the template surface were measured by BET surface area analysis (see Supporting method S7) and a result is described in Fig. 5(A). The surface area achieved from the analysis is 183 m^2/g. The value is relatively higher than that of value (160 m^2/g) indicated by Vera-Robles et al. (2015), but lower than of measured value (341.57 m^2/g) from Mao et al. (2012). The variation could be interpreted by the length of a material that made of mesoporous structures. The pore sizes in the template were determined around 35–40 nm that is suitable for decoration of Au-MNS via thiol moieties. Moreover, immunogold colloids to the specific biomarkers that are present on the templates were characterized by SEM for Au-MNS colloids and SERS-tags in Fig. 4 (S) and Fig. 5(B), respectively. The approximate values of pore diameter from SEM image showed that Au-MNS and SERS-tags were formed on the phage-based mesoporous template can be used as a SERS substrate for diagnostics.

3.4. SERS-based triplex assay of sepsis-specific biomarkers

The 50 μl of 1 mM SERS-tags for each corresponding target antigen was added to human serum containing sepsis-specific biomarkers for 30 min, the free biomarkers were removed by centrifugation. 200 μl of the suspensions of the magnetic templates in PBS was added to the SERS-tags bearing sepsis-specific biomarkers and incubated to form sandwich structured complexes involving the SERS-tag/biomarker/magnetic template via antibody/antigen interaction for 30 min The final resultants containing the target complexes were separated by a magnet to eliminate the free SERS-tags after washing five times. SERS measurement was conducted by a procedure as described in Supporting method S6. Since SERS intensity is not only dependent on the species of the SERS active molecule, but also on the direction light polarization and wavelength of the incident light (Seung et al., 2008), we used a linear polarizer (PRM1/M, Thorlabs) to control the polarization direction of the incident laser light (785 nm). In case of dimer, the highest Raman intensity is obtained for an incident polarization parallel to the dimer axis (Xu and Käll, 2003). However, SERS-based immunoassays compose of more than two nanoparticles as a cluster, the polarization dependency turned out to be in all polarization angles more isotropic than for the dimer axis of isolated dimers, which is as a result of a complicated electromagnetic coupling cluster nanoparticles (Xu and Käll, 2003) called “hot spots”.

In sepsis detection, Fig. 6(A) presents a triplex assay of CRP, PCT, and sTREM-1 corresponding to ATP, R6G and TAMRA Raman dyes that were used for the specific SERS-tags, respectively. According to the recorded spectra, multi-peaks for 4-ATP, R6G, and TAMRA spectra appear in the triplex assay were equivalent to those in the single assay. These results also showed that the three targets did not interfere with each other in the SERS-based immunoassay

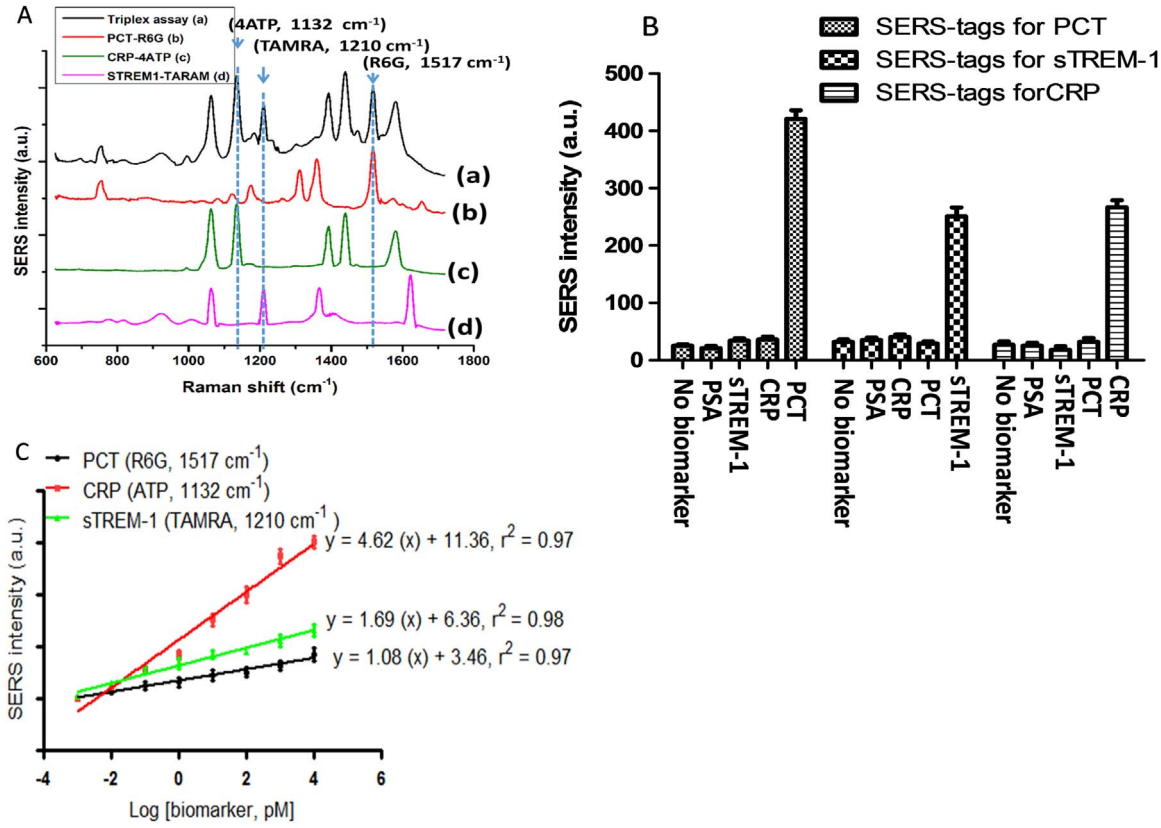

Fig. 6. Triplex detection for sepsis. (A) SERS spectra of Raman dyes corresponding to the specific targets on the template. (B) Detection of unspecific and cross-talk assay for the biomarker-based sepsis. (C) Linear fitting of the peak intensities of 1517 cm^{-1}, 1132 cm^{-1}, and 1210 cm^{-1} as a function of concentration of PCT, CRP, and sTREM-1, respectively. Error bars denote the standard deviations achieved from three independent measurements.

system. Since we considered that unspecific bindings may occur throughout the experiment, the incubation of prostate-specific antigen (PSA) with the complex of the SERS-tag and the magnetic template was handled individually. Unspecific interactions between SERS-tags and the magnetic template in the absence of the biomarkers or crosstalk between the antigens and antibodies were also observed (Fig. 6(B)). The typical SERS peaks did not appear in the corresponding SERS spectra, which indicate that no sandwich structured complexes, showed high specificity of the assay.

We used the concentration range of 1 pM to 1 nM to determine the limit of detection (LOD) for each biomarker in the assay. The concentration-based SERS spectra of the average value from three SERS scans are shown in Fig. 6(C). This describes the linear correlation between the typical peaks of ATP (1087 cm^{-1}), R6G (1363 cm^{-1}) and TAMRA (1650 cm^{-1}) and the concentration of CRP, PCT and STREM-1, respectively. The regression equations are $y=4.62(x)+11.36$ ($r^2=0.97$), $y=1.69(x)+6.36$ ($r^2=0.98$), and $y=1.08(x)+3.46$, $r^2=0.97$ for CRP, STEM-1, and PCT, respectively. The LOD for each biomarker in the triplex assay is calculated using the lowest concentration that can be detected in a signal three times higher than the standard deviation of the blank control (PSA antigen). The LOD values were determined to be 27 pM, 103 pM, and 78 pM for CRP, PCT, and sTREM-1, respectively. These LOD values were sensitivity enough compared to the biomarker concentration in patients with sepsis (Schmit and Vincent, 2008).

4. Conclusions

We developed a new SERS substrate based on display of cysteine-rich peptide on M13 phages. The cysteine moieties on M13 phages as a thiol donor without a need of chemical modifications were reduced to generate the active thiol moieties and then polymerized with silica precursors to form the amorphous biomaterial gel. The polymer was calcinated to from mesoporous template to anchor the Au-MNS via thiol-gold interactions to form the magnetic mesoporous structures. The magnetic template was characterized with TEM, SEM, FTIR, BET, and Raman scattering techniques. The magnetic template was applied for sepsis detection by using specific antibodies to capture sepsis-specific biomarkers. A triplex assay of CRP, PCT, and sTREM-1 in human serum shows good specificity and sensitivity, with low LODs at 27 pM, 103 pM, and 78 pM for CRP, PCT, and sTREM-1, respectively. Therefore, SERS-based triplex assays on magnetic templates can be a promising alternative method for early clinical diagnosis of sepsis. Finally, the mesoporous structure developed by M13 phage can also be applied for SERS substrate, catalysis, and thiol-redox assembly for drug delivery in biomedical applications.

Acknowledgements

This study was supported by the National Research Foundation of Korea (NRF) grants (NRF-2013R1A2A1A01015644/2010–0027955) and the grants (2014M1A8A1049278) from Korea Carbon Capture and Sequestration (CCS) R&D Centre of the National Research Foundation (NRF) of the Ministry of Science, ICT, and Future Planning of Korea.

Appendix A. Supplementary material

Supplementary data associated with this article can be found in the online version at http://dx.doi.org/10.1016/j.bios.2016.05.043.

References

Abu Hatab, N.A., Oran, J.M., Sepaniak, M.J., 2008. ACS Nano 2, 377–385.
Blaik, R.A., Lan, E., Huang, Y., Dunn, B., 2016. ACS Nano 10, 324–332.
Brolo, A.G., 2012. Nat. Photonics 6, 709–713.
Calandra, T., Cohen, J., 2005. Crit. Care Med. 22, 1538–1548.
Chung, W.J., Lee, D.Y., Yoo, S.Y., 2014. Int. J. Nanomedicine 9, 5825–5836.
Ghosh, D., Lee, Y., Thomas, S., Kohli, A.G., Yun, D.S., Belcher, A.M., Kelly, K.A., 2012. Nat Nanotechnol. 7, 677–682.
Groen, J.C., Peffer, L.A.A., Pérez-Ramírez, J., 2003. Microporous Mesoporous Mater. 60, 1–17.
Gibot, S., Béné, M.C., Noel, R., Massin, F., Guy, J., Cravoisy, A., Barraud, D., De Carvalho Bitten-court, M., Quenot, J.P., Bollaert, P.E., Faure, G., Charles, P.E., 2012. Am. J. Respir. Crit. Care Med. 186, 65–71.
Hall, W.P., Ngatia, S.N., Van Duyne, R.P., 2011. J. Phys. Chem. C. Nanomater. Interfaces 115, 1410–1414.
Huang, Y., Cai, H., Feng, D., Gu, D., Deng, Y., Tu, B., Wang, H., Webley, P.A., Zhao, D., 2008. Chem. Commun 23, 2641–2643.
Huh, Y.S., Chung, A.J., Erickson, D., 2009. Microfluid Nanofluid 6, 285–297.
Joseph, V., Matschulat, A., Polte, J., 2011. J. Raman Spectrosc. 42, 1736–1742.
Kingma, K.J., Hemley, R.J., 1994. Am. Mineral 79, 269–273.
Li, K., Chen, Y., Li, S., Nguyen, H.G., Niu, Z., You, S., Mello, C.M., Lu, X., Wang, Q., 2010. Bioconjug. Chem. 21, 1369–1377.
Mao, C., Wang, F., Cao, B., 2012. Angew. Chem. Int. Ed. Engl. 51, 6411–6415.
Nguyen, A.H., Lee, J.U., Sim, S.J., 2015a. J. Opt. 17 (114022), 12.
Nguyen, A.H., Lee, J., Choi, H.I., Kwak, H.S., Sim, S.J., 2015b. Biosens. Bioelectron. 70, 358–365.
Nguyen, A.H., Ma, X., Sim, S.J., 2015c. Biosens. Bioelectron. 66, 497–503.
Oh, Y.K., Hong, L.Y., Asthana, Y., Kim, D.P., 2006. J. Ind. Eng. Chem. 6, 911–917.
Pokorski, J.K., Steinmetz, N.F., 2011. Mol. Pharm. 8, 29–43.
Rascher, D., Geerlof, A., Kremmer, E., Krämer, P., Schmid, M., Hartmann, A., Rieger, M., 2014. Biosens. Bioelectron. 59, 251–258.
Reinhart, K., Bauer, M., Riedemann, N.C., Hartog, C.S., 2012. Clin. Microbiol. Rev. 25, 609–634.
Rittirsch, D., Flier, M.A., Ward, P.A., 2008. Nat. Rev. Immunol. 8, 776–787.
Schmit, X., Vincent, J.L., 2008. Clin. Microbiol. Infect. 36, 213–219.
Seung, J.L., Jeong, M.B., Moskovits, M., 2008. Nano Lett. 8, 3244–3247.
Sharma, B., Cardinal, M.F., Kleinman, S.L., Greeneltch, N.G., Frontiera, R.R., Blaber, M. G., Schatz, G.C., Van Duyne, R.P., 2013. Mater. Res. Bull. 38, 615–623.
Sharma, B., Frontiera, R.R., Henry, A.I., Ringe, E., Richard, P., Van Duyne, R.P., 2012. Mater. Today 15, 16–25.
Smith, G.P., 1985. Science 228, 1315–1317.
Sutherland, A., Thomas, M., Brandon, R.A., Brandon, R.B., Lipman, J., Tang, B., McLean, A., Pas-coe, R., Price, G., Nguyen, T., Stone, G., Venter, D., 2011. Crit, Care. 15, R149.
Swift, B.M., Denton, E.J., Mahendran, S.A., Huxley, J.N., Rees, C.E., 2013. J. Microbiol Methods 94, 175–179.
Tian, R., Seitz, O., Li, Meng, Hu, W., Chabal, Y.J., GAO, J., 2010. Langmuir 26, 4563–4566.
Tsvetkov, M.Y., Khlebtsoc, B.N., Khandadeev, V.A., Bagratashvili, V.N., Timashev, P.S., Samoylovich, M.I., Khlebtsov, N.G., 2013. Nanoscale Res. Lett. 8, 250–257.
Vera-Robles, L.I., González-Gracida, J., Hernández-Gordillo, A., Campero, A., 2015. Langmuir 31, 9188–9197.
Xu, H., Käll, M., 2003. Chem Phys Chem 4, 1001–1005.
Yang, T., Guo, X., Wang, H., Fu, S., Wen, Y., Yang, H., 2015. Biosens. Bioelectron. 68, 350–357.
Zakariah, A.N., Cozzi, S.M., Van Nuffelen, M., Clausi, C.M., Pradier, O., Vincent, J.L., 2008. Crit. Care Med. 36, 1507–1512.
Zhang, B., Davis, S.A., Mann, S., 2002. Chem. Mater. 14, 1369–1375.